ChemComm

Square-planar Co(III) in {O4} Coordination: Large ZFS and Reactivity with ROS

Journal:	*ChemComm*
Manuscript ID	CC-COM-06-2018-004464.R2
Article Type:	Communication

Journal Name

COMMUNICATION

Square-planar Co(III) in {O_4} Coordination: Large ZFS and Reactivity with ROS

Received 00th January 20xx,
Accepted 00th January 20xx

DOI: 10.1039/x0xx00000x

www.rsc.org/

Jennifer L. Steele,[a] Laleh Tahsini,[a] Chen Sun,[a] Jessica K. Elinburg,[a] Christopher M. Kotyk,[a] James McNeely,[a] Sebastian A. Stoian,[b] Alina Dragulescu-Andrasi,[d] Andrew Ozarowski,[c] M. Ozerov,[c] J. Krzystek,[c] Joshua Telser,[f] Jeffrey W. Bacon,[a] James A. Golen,[e] Arnold L. Rheingold,[e] and Linda H. Doerrer[a, *]

Oxidation of distorted square-planar perfluoropinacolate Co compound $[Co^{II}(pin^F)_2]^{2-}$, 1, to $[Co^{III}(pin^F)_2]^{1-}$, 2, is reported. Rigidly square-planar 2 has an intermediate-spin, $S = 1$, ground state and very large zero-field splitting (ZFS) with $D = 67.2\ cm^{-1}$; $|E| = 18.0\ cm^{-1}$ (E/D) = 0.27, $g_\perp = 2.10$, $g_\parallel = 2.25$ and $\chi_{TIP} = 1950 \cdot 10^{-6}\ cm^3/mol$. This Co(III) species, 2, reacts with ROS to oxidise two $(pin^F)^{2-}$ ligands to form tetrahedral $[Co^{II}(Hpfa)_4]^{2-}$, 3.

Metal complexes supported by oxidatively robust ligands are crucial to many catalytic transformations including water remediation,[1] water oxidation,[2-4] and selective C-H bond oxidation.[5-8] One approach that engenders oxidative resistance is to use extensively fluorinated ligands. Chelating bidentate ligands have additional stability vs. two monodentate ligands, and H_2pin^F, perfluoropinacol, is of particular interest because its complexes can routinely be prepared in water ($pKa_1 = 6.05$, $pKa_2 = 10.7$, titration in Figure S1). Homoleptic 3*d* complexes $[M(pin^F)_2]^{2-}$ with M = Fe - Zn have been reported[9, 10] including $[Me_4N]_2[Co(pin^F)_2]$, **1** (Scheme 1), which binds CH_3CN but not THF in solution.[10] Reactivity with O_2 for this Co species was also reported,[11] the conclusions from which we have come to doubt as discussed below.

Compound **1** is stable for days in aqueous solutions as the five coordinate adduct $[Co(OH_2)(pin^F)_2]^{2-}$ when buffered between pH 9 – 11 with $(pin^F)^{2-}$.[12] In contrast, CH_3CN solutions of **1** in air undergo distinct colour changes in hours. The pink **1** (λ_{max}, nm (ε, $M^{-1}cm^{-1}$)) = 505 (27), 560 (43)), converts to a bright yellow/orange species with an intense absorption at 405 nm (3790), **2**, and then ultimately transforms to a violet species, **3** (λ = 481 (133), 567 (165)) in ~ 95% yield after five days (Figure S2). Purple X-ray quality crystals were obtained by layering Et_2O onto violet acetone solutions, enabling identification of the pseudo-tetrahedral complex $[Me_4N]_2[Co^{II}(Hpfa)_4]$, **3**. The metal centre is bound by four monodentate alkoxide ligands, designated $(Hpfa)^-$ for the monodeprotonated form of the perfluoroacetone geminal diol, H_2pfa (Scheme 1 and Figure 1). As noted, the conversion of **1** to **3** in CH_3CN under aerobic conditions passes through an orange intermediate, **2**, with a strong absorbance at 405 nm. Efforts to isolate the orange species from this reaction mixture were unsuccessful. The composition of **3** suggests that four equiv of hydroxyl radical, $HO^\bullet$, are formally required for its formation. Therefore, we treated **1** with H_2O_2 trying to prepare a posited {Co(III)-OH} species. Adding one equiv of H_2pin^F to **1** in wet CH_3CN, followed by one equiv of H_2O_2, affords an absorbance increase at 405 nm over an hour (Figure 2). Next, the ligand-cleaved product **3** can be formed by adding one equiv of Me_4NOH to **2** following its full formation (Figure S3). Isolation

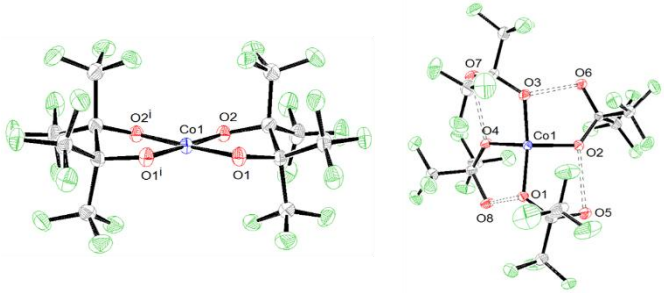

Figure 1. ORTEPs of anions of **2** (left) and **3** (right). Dotted lines indicate hydrogen bonding interactions.

[a] *Chemistry Department, Boston University, 590 Commonwealth Ave., Boston, MA 02139 USA.*
[b] *Department of Chemistry, University of Idaho, 875 Perimeter Drive, MS 2343, Moscow, ID 83844, USA*
[c] *National High Magnetic Field Laboratory, Florida State University, 1800 E. Paul Dirac Drive, Tallahassee, FL 32310, USA*
[d] *Department of Chemistry and Biochemistry, Florida State University, 95 Chieftan Way, Tallahassee, FL 32306, USA*
[e] *Department of Chemistry and Biochemistry, University of California, San Diego, 9500 Gilman Drive, MC 0332, La Jolla, CA 92093, USA.*
[f] *ƒ Department of Biological, Chemical and Physical Sciences, Roosevelt University, Chicago, IL 60605, USA*
† Footnotes relating to the title and/or authors should appear here.
Electronic Supplementary Information (ESI) available including the Experimental Section and CIFs for **2** (1407677) and **3** (1407676) via the CCDC. See DOI: 10.1039/x0xx00000x
† Footnotes relating to the title and/or authors should appear here.
Electronic Supplementary Information (ESI) available: [details of any supplementary information available should be included here]. See DOI: 10.1039/x0xx00000x

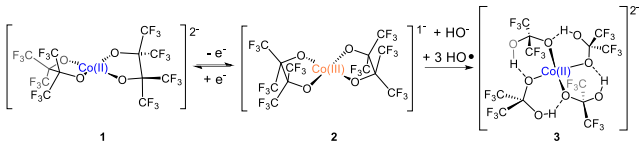

Scheme 1. Formal interconversions of anions $[Co(pin^F)_2]^{2-}$, **1**, $[Co(pin^F)_2]^{1-}$, **2**, and $[Co(Hpfa)_4]^{2-}$, **3**

of a posited Co(III) intermediate was not achieved from this reaction, due to an additional pathway that led to an insoluble brown solid and complete loss of product after 24 h. Conversion of **1** to **2** occurs at a faster rate in the presence of larger amounts of hydrogen peroxide.

Analytically pure **2** was obtained by oxidizing **1** under N_2 with $AgPF_6$ in THF/CH_3CN to yield the surprising square-planar Co(III) species $[Me_4N][Co^{III}(pin^F)_2]$. The UV-vis spectrum of **2** has an LMCT band at λ_{max} = 405 nm (ε = 3790 $M^{-1}cm^{-1}$). The solution-based, Evans method[13-15] room-temperature magnetic moment of 3.63 μ_B for **2** suggests an S = 1, intermediate-spin state. This observation is consistent with other Co(III) square planar compounds with $\{N_4\}$,[16-19] $\{S_4\}$,[20, 21] $\{C_4\}$,[22] and heteroleptic[23] coordination (summary in Table S1). X-ray quality crystals were obtained by layering a THF solution onto CH_2Cl_2 (Figure 1 and Table S3). The square planar coordination with τ_4 = 0.03 has Co-O bond lengths (1.8020(17) and 1.7995(18) Å) shorter than the average (1.962(3) Å) in **1**, as expected.[10] Notably, the UV-vis spectra in both coordinating and non-coordinating solvents are virtually identical (Figure S4), indicating that there is no axial ligand bound in **2** in solid state or in solution. Even when hydroxide is added to **2**, no coordination is observed, suggesting a steric, not electronic, reason for unsaturation. The combination of shorter Co-O bonds and the steric bulk of eight CF_3 groups is proposed to inhibit coordination of a fifth ligand.

Addition of O_2 to $[^nBu_4N]_2[Co(pin^F)_2]$ in "acidified" solution has previously been reported to give a product with a λ_{max} of 405 nm.[11] Therein the product was proposed to be the high-spin cobalt(II) species $[^nBu_4N][Co(pin^F)(Hpin^F)(O_2)]\cdot EtOH$ based on a solution magnetic moment measurement and EPR data.[11] Our attempts to repeat the isolation of this product by this method have proved unsuccessful. Because **2** has an identical λ_{max}, similar light sensitivity, and similar magnetic moment to that reported earlier,[11] we suggest that the proposed formula[11] is incorrect, and that the previously reported compound was $(^nBu_4N)^+$ salt of $[Co^{III}(pin^F)_2]^{1-}$.

Compound **2** incorporates a rare, paramagnetic Co(III) ion. The room-temperature ^{1}H-NMR-derived magnetic moment of **2** is corroborated by SQUID magnetometry on a solid sample. Figure 3 shows χT ~ 1.8 $cm^3\cdot K/mol$ at 300 K corresponding to an apparent effective magnetic moment of 3.78 μ_B. These values are intermediate between those expected for a triplet ($\chi T \approx 1$ $cm^3\cdot K/mol$) and a quintet spin state ($\chi T \approx 3$ $cm^3\cdot K/mol$). From 300 to 50 K, χT gradually decreases, followed by a more dramatic fall to nearly zero at very low temperature. This behaviour suggests the presence of a large temperature independent paramagnetic (TIP) contribution and a large zero-field splitting (ZFS) at low temperature. Least squares fitting of experimental data yielded a ZFS such that $|D|$ ~ 70 cm^{-1}, E/D ~ 1/3, g_{iso} = 2.24 and χ_{TIP} = $1950\cdot10^{-6}$ cm^3/mol. The observation of a triplet ground state with this large ZFS is corroborated by reduced magnetization data (inset of Figure 3 and Figure S5), and lack of an EPR signal regardless of temperature even for frequencies as high as 600 GHz ($h\nu$ = 20 cm^{-1}).[24] The ZFS was directly measured by FIRMS (Far InfraRed Magnetic Spectroscopy),[25] which detected two resonances in zero field at 49.2 cm^{-1} and 85.2 cm^{-1}, identified as D-E and D+E transitions, respectively (Figure 4) and leading to $|D|$ = 67.2 cm^{-1}; $|E|$ = 18.0 cm^{-1}. The 2E transition, which should appear at 36 cm^{-1}, was not observed and therefore the sign of D is likely to be positive. The positive sign of D is also supported by magnetic fits (Figure S5) and is predicted by second-order perturbation theory using the electronic structure discussed below. Together these observations reveal a large unquenched orbital momentum and a spin-orbit mixing of the orbital ground state with several low–lying orbital states.

Figure 2. UV-vis spectral changes of conversion of **1** to **2** effected by H_2O_2 in CH_3CN solution. Inset shows the time course of this process.

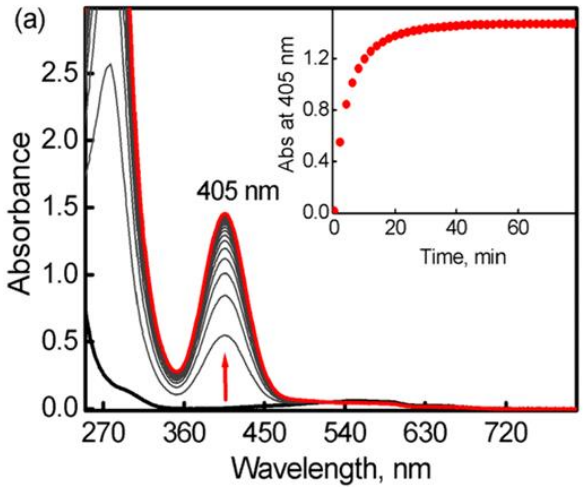

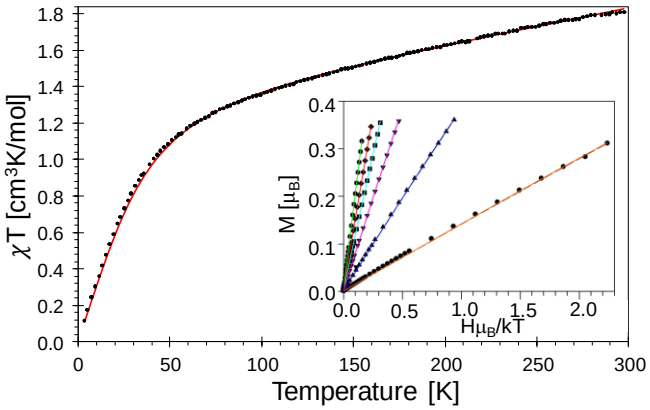

Figure 3. Plot of χT vs. temperature recorded for a powder sample of **2**. Shown in black are experimental data points. The solid red line is a simulation obtained for S = 1 with D = 70 cm^{-1}, E/D = 0.33, g_{iso} = 2.24, and χ_{TIP} = $1950\cdot10^{-6}$ cm^3/mol. The inset shows the reduced magnetization data recorded at 1.7 K, 5 K, 10 K, 15 K, 20 K, and 30 K for fields from 0 to 7 T. The solid lines are simulations obtained using D = 65.44 cm^{-1}, E/D = 0.33, g_{iso} = 2.22.

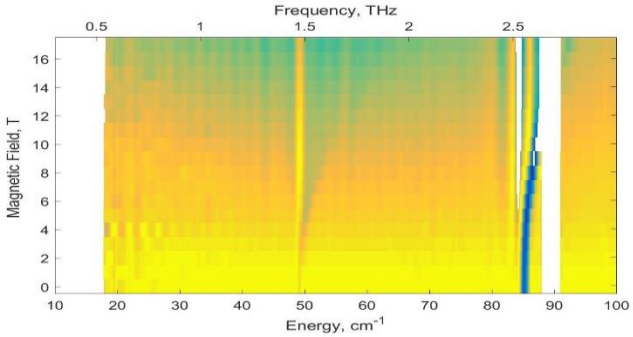

Figure 4. A false colour map of FIRMS resonances at 5 K showing two zero-field transitions at 49.2 cm^{-1} and 85.2 cm^{-1} evolving into powder patterns with applied magnetic field. More details can be found in Figures S6-7 in the SI.

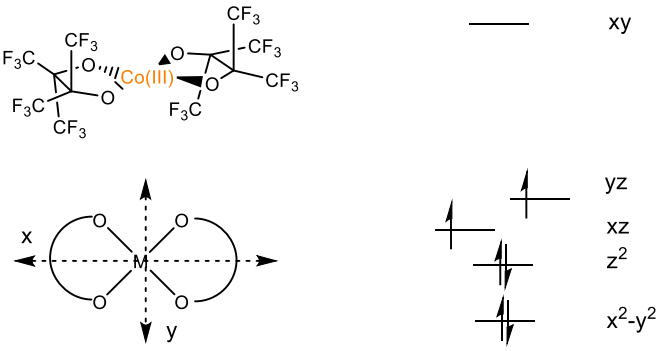

Scheme 2. Coordinate system used for the discussion of **2** along with a qualitative ligand field splitting diagram derived from NEVPT2(12,10) calculations averaged over three triplet states. NOs and NOONs can be found in Figure S26.

To illuminate the nature of the paramagnetic ground state and to rationalize the observed spectroscopic behaviour, we have completed a detailed theoretical investigation of **2**. Calculations using ORCA[26] revealed the ligand field splitting shown qualitatively in Scheme 2 (right).

An intermediate-spin, triplet ground state is further supported by triplet (**^{3}2**, 0.0 kcal/mol), singlet (**^{1}2**, 38.9 kcal/mol), and quintet (**^{5}2**, 15.8 kcal/mol) structures optimized at the PBE0/cc-pVTZ/RIJCOSX level of theory. These calculations not only yield a triplet configuration lowest in energy, but a geometry-optimized structure with the best structural agreement with **2** (Table S4). The spin density for **^{3}2** is localized on the Co atom (Figure S8) with the SOMOs best described as $3d_{xz}$ and $3d_{yz}$ orbitals. Analysis of the electron distribution suggests that the $3d_{z^2}$ and $3d_{x^2-y^2}$ orbitals are doubly occupied and that, to a first approximation, the $|(x^2-y^2)^2(z^2)^2(xz)^\alpha(yz)^\alpha|$ Slater determinant describes best the ground state of **2**. This electronic structure is confirmed by NEVPT2(12,10) calculations (Figure S14). The cobalt spin population was 1.80/1.94 in the PBE0/NEVPT2(12,10) calculations for **2** and 1.80/1.95 for **^{3}2** based on Löwdin population analysis. This result is a similar electronic structure to that reported in Co complexes with redox-active benzene dithiolate[27] and aminophenolate ligands.[28]

To predict magnetic properties, NEVPT2 calculations were performed on top of CASSCF(12,10) references averaged over the three lowest triplet roots for **2** (see ESI). The axial ZFS parameter *D*, rhombicity ratio *E/D*, and isotropic g-value were calculated to be 77.1 cm^{-1}, 0.27, and 2.37 respectively. These theoretical values compare well with experiment. The ***g***-tensor was calculated to be highly anisotropic with principal components g_z = 2.00, g_x = 2.43, and g_y = 2.67. The $^3B_2$ state (D_2 symmetry, 2273 cm^{-1}) is dominated by configurations characterized by $3d_{z^2}$ to $3d_{xz}$ (72.0%) and $3d_{x^2-y^2}$ to $3d_{xz}$ (22.1%) excitations. The $^3B_3$ state's (3802 cm^{-1}) dominant configurations are characterized by $3d_{z^2}$ to $3d_{yz}$ (72.0%) and $3d_{x^2-y^2}$ to $3d_{yz}$ (22.1%) excitations.

These quantum chemical theory calculations were complemented by a series of classical ligand field theory calculations[29] that determined $D \approx 70$ cm^{-1} with evidence that contributions from both quintet and singlet excited states are required for quantitative agreement with experiment, but the dominant contribution is from triplet excited states arising from transitions from the $3d_{z^2}$ and $3d_{x^2-y^2}$ orbitals to the $3d_{xz}$ and $3d_{yz}$ orbitals (details in ESI).

To understand the formation of **3** via **2**, **1** was reacted with O_2, H_2O, and H_2O_2. Compound **1** is stable up to pH = 11,[12] and therefore nucleophilic attack by hydroxide alone does not lead to C–C bond cleavage in neutral water; some oxidation is required. There is no appearance of **2** or conversion to **3** from the addition of H_2O or O_2 alone to **1**, but **1** reacts with O_2 in the presence of a mild acid such as H_2pin^F. This reaction slowly afforded **2**, but in significant yield only after four days, and complete conversion to **3** took seven days (Figure S17). When **2** in dry CH_3CN is exposed to air in the presence of $(^nBu_4N)PF_6$, it is slowly converted to **3** as indicated by UV-vis spectroscopy (Figure S18), with a competing pathway leading to an insoluble brown precipitate. Starting with dry CH_3CN and gradual exposure to air, the conversion from **2** to **3** takes up to a month and also shows conversion to a transient Co(II) species after 24 h. This Co(II) species could be **1**, which is produced from a solution of **2** when exposed to light under N_2 (Figure S18). These observations suggest that both the oxidant O_2 and a source of H^+ are necessary for the formation of **2,** and a further ROS is needed to form **3**. The fact that **2** does not form in H_2O suggests a radical species whose lifetime is greater in CH_3CN than H_2O.

Isotopic labelling experiments were conducted to determine the source of the new OH groups in the $(Hpfa)^-$ ligands. Each of $^{18}O_2$ and $H_2{}^{18}O$ was separately introduced to a solution of **1**, while the other component was kept unlabelled, and **3** formed in CH_3CN. The product **3** was recrystallized and analysed by ESI-MS (Figures S19-21) which showed ^{18}O in $[Co(Hpfa)_4]^{2-}$ from both reactions. These data and the H_2O_2 experiment suggest a reactive oxygen species, such as HO•, that can form in more than one way. Because oxidation is required, O_2 could be responsible for HO• formation, either indirectly from water oxidation, or directly from itself being converted to hydroxyl radical (Scheme S1).

Redox behaviour was also investigated with cyclic voltammetry (CV). Compound **1** showed a quasi-reversible Co^{3+}/Co^{2+} couple with an $E_{1/2}$ of -0.134 V vs Fc^+/Fc (Figure S22). Under N_2, **2** showed a reversible couple with an $E_{1/2}$ of -0.167 V vs. Fc/Fc^+, and when **3** was studied in dry CH_3CN under N_2, a widely-separated redox couple is observed, as well as another oxidation event (Figure S23).

The reactivity of these species was monitored by cyclic voltammetry: In CH_3CN under ambient conditions both electrochemical and UV-Vis data confirm the completion of the reaction of **1** to **3** within several hours (Figure S24). However, under ambient conditions in CH_3CN no conversion of purified **2** to **3** was observed within one day, which is consistent with our previously noted UV-Vis experiments

Interestingly, the CV of **3** in wet CH_3CN shows oxidative catalytic current (Figure S25), which increases with subsequent additions of H_2O until a solid blue precipitate forms. Controlled potential electrolysis, shows that the initial oxidative current significantly diminished after 750 s, and did not increase when H_2O was added at 1800 s. When the working electrode was placed in fresh electrolyte (Figures S26 and S27) little activity was observed indicating that there was not an active heterogeneous film. This catalytic activity may be water oxidation by nanoparticulate CoO_x material, a known H_2O oxidation catalyst,[30] for which **3** is a precursor in CH_3CN. Little change was observed in CV data when the solution was filtered (Figure S28).

In summary, a highly unusual square-planar, paramagnetic Co(III) species, $[Co(pin^F)_2]^{1-}$, **2**, has been prepared from $[Co(pin^F)_2]^{2-}$ by two different routes. Compound **2** has an intermediate-spin, $S = 1$, ground state and very large ZFS with $|D| \sim 70\ cm^{-1}$, $E/D \sim 1/3$, $g_\perp = 2.10$, $g_\parallel = 2.25$ and $\chi_{TIP} = 1950 \cdot 10^{-6}\ cm^3/mol$. This compound reacts with reactive oxygen species to form a new tetrahedral Co(II) compound, $[Co(Hpfa)_4]^{2-}$, **3**, encapsulated by four intramolecular hydrogen bonds among four monodentate diolate ligands.

This work was supported by NSF-CHE 1362550 (LHD), DOE-BES DE-FG02-11ER16253 (LHD), Boston University UROP, NSF-CHE 0619339 (BU NMR spectrometer). Part of this work was performed at NHMFL which is supported by the NSF award DMR-1644779 and by the State of Florida. Partial support for AD-A from the NSF (CHE 1464955) and the University of Idaho (SAS) is acknowledged. We thank the referees for useful mechanistic discussions.

Conflicts of interest

There are no conflicts to declare.

Notes and references

1. T. J. Collins and A. D. Ryabov, *Chem. Rev.*, 2017, **117**, 9140-9162.
2. H. Lv, Y. V. Geletii, C. Zhao, J. W. Vickers, G. Zhu, Z. Luo, J. Song, T. Lian, D. G. Musaev and C. L. Hill, *Chem. Soc. Rev.*, 2012, **41**, 7572-7589.
3. J. J. Concepcion, J. W. Jurss, M. K. Brennaman, P. G. Hoertz, A. O. T. Patrocinio, N. Y. Murakami Iha, J. L. Templeton and T. J. Meyer, *Acc. Chem. Res.*, 2009, **42**, 1954-1965.
4. P. Du and R. Eisenberg, *Energy Environ. Sci.*, 2012, **5**, 6012-6021.
5. R. A. Sheldon, I. W. C. E. Arends, G.-J. ten Brink and A. Dijksman, *Acc. Chem. Res.*, 2002, **35**, 774-781.
6. D. Wang, A. B. Weinstein, P. B. White and S. S. Stahl, *Chem. Rev.*, 2018, **118**, 2636-2679.
7. S. R. Neufeldt and M. S. Sanford, *Acc. Chem. Res.*, 2012, **45**, 936-946.
8. B. G. Hashiguchi, S. M. Bischof, M. M. Konnick and R. A. Periana, *Acc. Chem. Res.*, 2012, **45**, 885-898.
9. S. A. Cantalupo, S. R. Fiedler, M. P. Shores, A. L. Rheingold and L. H. Doerrer, *Angew. Chem., Int. Ed.*, 2012, **51**, 1000-1005.
10. L. Tahsini, S. E. Specht, J. S. Lum, J. J. M. Nelson, A. F. Long, J. A. Golen, A. L. Rheingold and L. H. Doerrer, *Inorg. Chem.*, 2013, **52**, 14050-14063.
11. C. J. Willis, *J. Chem. Soc., Chem. Commun.*, 1974, 117-118.
12. L. Tahsini, W. P. Carbery, M. Z. Ertem, S. A. Cantalupo, J. A. Golen, A. L. Rheingold, V. S. Batista and L. H. Doerrer, *manus in prep*, 2018.
13. G. A. Bain and J. F. Berry, *J. Chem. Educ.*, 2008, **85**, 532-536.
14. D. F. Evans, *J. Chem. Soc.*, 1959, 2003-2005.
15. S. K. Sur, *J. Magn. Reson.*, 1989, **82**, 169-173.
16. S. E. Harnung and E. Larsen, *Inorg. Chem.*, 2007, **46**, 5166-5173.
17. B. Ramdhanie, L. N. Zakharov, A. L. Rheingold and D. P. Goldberg, *Inorg. Chem.*, 2002, **41**, 4105-4107.
18. L. H. Doerrer, M. T. Bautista and S. J. Lippard, *Inorg. Chem.*, 1997, **36**, 3578-3579.
19. P. J. M. W. L. Birker, J. J. Bour and J. J. Steggerda, *Inorg. Chem.*, 1973, **12**, 1254-1259.
20. R. Williams, E. Billig, J. H. Waters and H. B. Gray, *J. Am. Chem. Soc.*, 1966, **88**, 43-50.
21. F. L. Benedito, T. Petrenko, E. Bill, T. Weyhermüller and K. Wieghardt, *Inorg. Chem.*, 2009, **48**, 10913-10925.
22. M. A. García-Monforte, I. Ara, A. Martín, B. Menjón, M. Tomás, P. J. Alonso, A. B. Arauzo, J. I. Martínez and C. Rillo, *Inorg. Chem.*, 2014, **53**, 12384-12395.
23. P. O. Lagaditis, B. Schluschaß, S. Demeshko, C. Würtele and S. Schneider, *Inorg. Chem.*, 2016, **55**, 4529-4536.
24. A. K. Hassan, L. A. Pardi, J. Krzystek, A. Sienkiewicz, P. Goy, M. Rohrer and L.-C. Brunel, *J. Magn. Reson.*, 2000, **142**, 300-312.
25. J. Ludwig, Y. B. Vasilyev, N. N. Mikhailov, J. M. Poumirol, Z. Jiang, O. Vafek and D. Smirnov, *Phys. Rev. B*, 2014, **89**, 241406.
26. F. Neese, *ORCA – An Ab Initio, DFT and Semiempirical SCF-MO Package, Ver. 4.0*, Max Planck Institute for Chemical Energy Conversion, Mülheim a. d. Rurh, Germany, 2017, pp.
27. K. Ray, A. Begum, T. Weyhermüller, S. Piligkos, J. van Slageren, F. Neese and K. Wieghardt, *J. Am. Chem. Soc.*, 2005, **127**, 4403-4415.
28. B. Eckhard, E. Bothe, P. Chaudhuri, K. Chlopek, D. Herebian, S. Kokatam, K. Ray, T. Weyhermüller, F. Neese and K. Wieghardt, *Chemistry – A European Journal*, 2005, **11**, 204-224.
29. J. Bendix, in *Comprehensive Coordination Chemistry II, Volume 2: Fundamentals: Physical Methods, Theoretical Analysis, and Case Studies*, ed. A. B. P. Lever, Elsevier, Amsterdam, 2003, vol. 2, pp. 673-676.
30. X. Deng and H. Tuysuz, *ACS Catalysis*, 2014, **4**, 3701-3714.

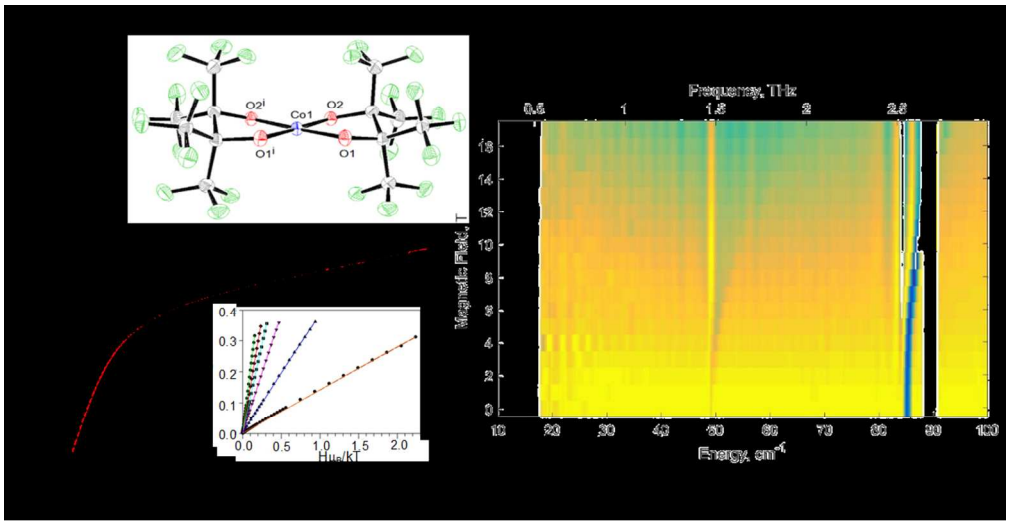
O2i
Co1
O2
O1i
O1
0.4
0.3
0.2
0.1
0.0
0.0
0.5
1.0
1.5
2.0
Frequency, THz
0.5
1
1.5
2
2.5
Magnetic Field, T
18
14
12
10
8
6
4
2
0
10
20
30
40
50
60
70
80
90
100
Energy, cm-1